JARO 16: 727–745 (2015)
DOI: 10.1007/s10162-015-0539-3

JARO
Journal of the Association for Research in Otolaryngology

Research Article

Towards a Diagnosis of Cochlear Neuropathy with Envelope Following Responses

Luke A. Shaheen,[1,2] Michelle D. Valero,[2,3] and M. Charles Liberman[1,2,3]

[1]*Program in Speech and Hearing Bioscience and Technology, Harvard-MIT Division of Health Sciences and Technology, Cambridge, MA 02139, USA*

[2]*Eaton-Peabody Laboratories, Massachusetts Eye and Ear Infirmary, Boston, MA 02114, USA*

[3]*Department of Otology and Laryngology, Harvard Medical School, Boston, MA 02115, USA*

Received: 26 February 2015; Accepted: 9 August 2015; Online publication: 1 September 2015

ABSTRACT

Listeners with normal audiometric thresholds can still have suprathreshold deficits, for example, in the ability to discriminate sounds in complex acoustic scenes. One likely source of these deficits is cochlear neuropathy, a loss of auditory nerve (AN) fibers without hair cell damage, which can occur due to both aging and moderate acoustic overexposure. Since neuropathy can affect up to 50 % of AN fibers, its impact on suprathreshold hearing is likely profound, but progress is hindered by lack of a robust non-invasive test of neuropathy in humans. Reduction of suprathreshold auditory brainstem responses (ABRs) can be used to quantify neuropathy in inbred mice. However, ABR amplitudes are highly variable in humans, and thus more challenging to use. Since noise-induced neuropathy is selective for AN fibers with high thresholds, and because phase locking to temporal envelopes is particularly strong in these fibers, the envelope following response (EFR) might be a more robust measure. We compared EFRs to sinusoidally amplitude-modulated tones and ABRs to tone-pips in mice following a neuropathic noise exposure. EFR amplitude, EFR phase-locking value, and ABR amplitude were all reduced in noise-exposed mice. However, the changes in EFRs were more robust: the variance was smaller, thus inter-group differences were clearer. Optimum detection of neuropathy was achieved with high modulation frequencies and moderate levels. Analysis of group delays was used to confirm that the AN population was dominating the responses at these high modulation frequencies. Application of these principles in clinical testing can improve the differential diagnosis of sensorineural hearing loss.

Keywords: hidden hearing loss, auditory neuropathy, acoustic overexposure, envelope following response, auditory steady-state response, auditory brainstem response, auditory nerve

INTRODUCTION

Moderate noise exposure can cause a rapid loss of synapses between cochlear hair cells and auditory nerve (AN) terminals, followed by a slow degeneration of AN cell bodies and central axons (Kujawa and Liberman 2009; Lin et al. 2011). This neuropathy can occur without damage to hair cells, and despite full recovery of thresholds for distortion product otoacoustic emissions (DPOAEs) and auditory brainstem responses (ABRs). In normal ears, from 10 to 30 AN fibers synapse on each inner hair cell (IHC), depending on species and cochlear location (Liberman et al. 1990; Maison et al. 2013b) and these fibers can be divided into functional subgroups based on spontaneous discharge rate (SR) and sensitivity to sound (Liberman 1978). The SR distribution is bimodal, with roughly 40 % in the low-rate peak (SR < about 18 spikes/s) and 60 % in the high-rate peak. Single-fiber recordings in

Correspondence to: Luke A. Shaheen · Eaton-Peabody Laboratories · Massachusetts Eye and Ear Infirmary · Boston, MA 02114, USA. Telephone: (845) 532 0825; email: lshaheen@mit.edu

guinea pig suggest that noise-induced neuropathy is selective for high-threshold, low-SR fibers, and that the remaining low-threshold, high-SR fibers exhibit normal responses (Furman et al. 2013). This helps explain why noise-induced cochlear neuropathy can have no discernible effect on ABR thresholds, which must rely only on high-SR fiber responses since low-SR fibers are unresponsive at low stimulus levels (Liberman 1978).

Post-mortem studies suggest that AN primary degeneration may be widespread in humans (Makary et al. 2011), but it is currently undetected by routine clinical examination. Work in animals shows that more than 80 % of the AN fiber population can be silenced without shifting behavioral thresholds for tones in quiet, so long as the outer hair cell (OHC) amplifier is intact (Lobarinas et al. 2013). The impact of such primary neural degeneration on suprathreshold hearing ability is likely profound, but not well understood. A prerequisite for diagnosing this "hidden hearing loss" is a robust test for neuropathy suitable for use in humans. In animal studies, changes in suprathreshold amplitudes of ABR wave I are well correlated with cochlear neuropathy, so long as the cochlear amplifier is undamaged (Kujawa and Liberman 2009).

However, the envelope following response (EFR), the far-field response to an amplitude-modulated tone (Rickards and Clark 1972; Campbell et al. 1977; Kuwada et al. 1986), may provide a more robust metric of neuropathy than ABR. Human studies have documented a strong correlation between EFR and ABR thresholds (Stapells et al. 1987; Johnson and Brown 2005; D'haenens et al. 2009). The EFR, and related measures such as the steady-state response to synthetic vowels, have also been investigated at suprathreshold levels: reduced responses in listeners with normal audiograms have been associated with deficits detecting signals in noise (Dimitrijevic et al. 2004), using temporal cues (Ruggles et al. 2011), and in modulation and interaural-time-delay thresholds (Bharadwaj et al. 2015). One possible cause of these deficits may be partial cochlear neuropathy of the sort documented histologically in noise-exposed animals (Kujawa and Liberman 2009; Furman et al. 2013; reviewed in Bharadwaj et al. 2014) and aging animals (Sergeyenko et al. 2013).

To the extent that they are dominated by AN fibers, EFRs might be particularly sensitive to noise-induced neuropathy, because low-SR AN fibers show greater synchronization than high-SR fibers to sinusoidally amplitude-modulated (SAM) tones (Joris and Yin 1992), especially at moderate-to-high stimulus levels (Fig. 1B). In contrast, ABRs are evoked by transient stimuli and dominated by onset responses, which are relatively small in low-SR fibers (Rhode and Smith 1985; Taberner and Liberman 2005; Fig. 1A). Thus, the low-SR contribution to the ABR is disproportionately low (Bourien et al. 2014). In addition, phase information can be extracted from EFRs, and measures of phase-locking value (PLV) might be more robust to human anatomical variations (Gorga et al. 1988; Nikiforidis et al. 1993) that complicate amplitude measures in both electrophysiological tests.

In this study, we compare EFRs and ABRs in mice with selective low-SR neuropathy after noise exposure. We contrast this etiology with one affecting all SR groups: mutant mice lacking the large-conductance voltage and Ca^{2+}-activated K^+ (BK) channel expressed in hair cells and AN fibers (Skinner et al. 2003; Hafidi et al. 2005). In this model, OHC function is normal, but AN fiber firing rates are decreased regardless of SR (Oliver et al. 2006), due to an increase in the IHC time constant, which decreases spike synchronization at stimulus onset, and an increase in the AN refractory period, which directly affects maximum rate.

EFR amplitude and PLV were reduced in both noise-exposed and BK knockout (KO) mice, as was the amplitude of ABR wave I. However, the two pathologies caused different patterns of reduction vs. stimulus level in ways consistent with the different subgroups of AN fibers affected. We found an optimum range of EFR modulation frequencies where sensitivity to AN loss is maximal (~1 kHz), below which responses are increasingly dominated by a mixture of sources, and above which responses are dominated by hair cell potentials. In both models, the EFR data outperformed the ABR data with respect to the sensitivity and specificity for the detection of pathology.

METHODS

Animals and Groups

Male CBA/CaJ mice were exposed awake and unrestrained to octave-band noise (8–16 kHz) for 2 h, within a cage suspended directly below the horn of the loudspeaker in a small, reverberant chamber. Noise calibration to target sound pressure level (SPL) was performed immediately before each exposure session. Control mice were of the same age, gender, and strain, but were not exposed to the noise. Three different groups were used, each with their own age-matched controls: group 1a—exposed to 98 dB SPL at 8 weeks of age, (4 control, 5 exposed); group 1b—also exposed to 98 dB SPL at 8 weeks (6 control, 6 exposed); and group 2—exposed to

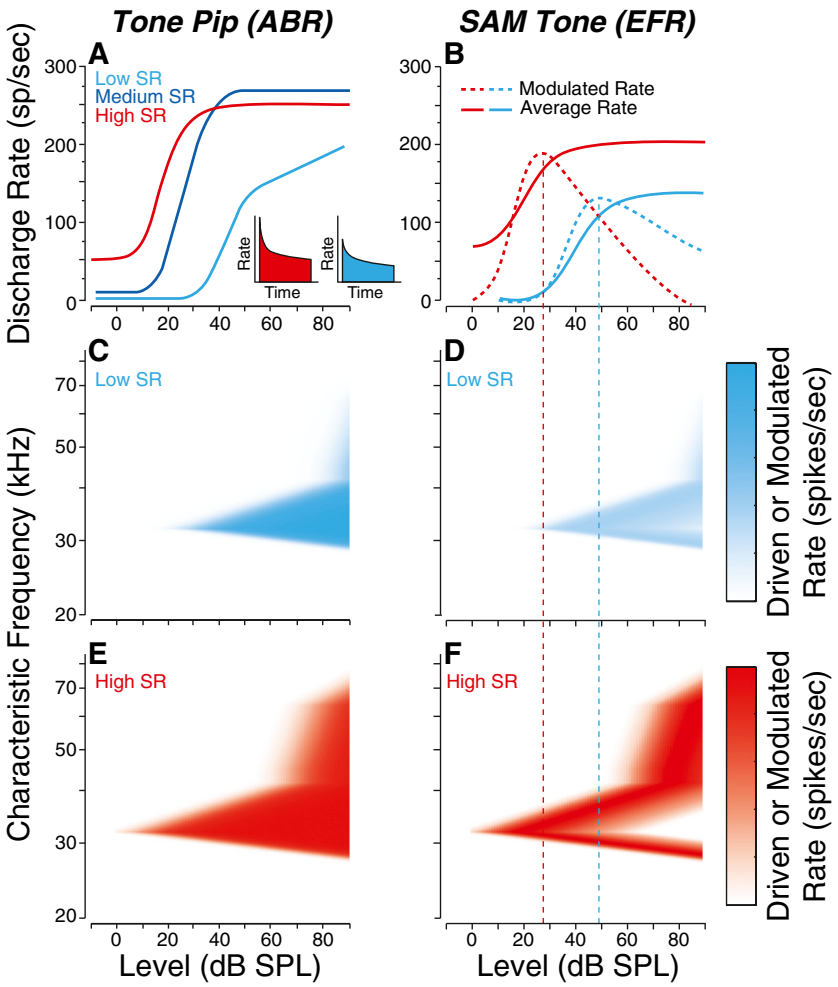

FIG. 1. Schematics of AN responses according to SR group. **A** Rate vs. level functions for high-, medium-, and low-SR fibers to tone bursts at the characteristic frequency (Liberman 1978). The *insets* show post-stimulus time histograms of the response to a moderate-level tone burst: onset rates are higher in the high-SR fiber than in the low-SR fiber (Taberner and Liberman 2005). **B** Responses to SAM tones in high- vs. low-SR fibers expressed as average rate and modulated rate. Responses are to carrier tones at the characteristic frequency, amplitude modulated at 100 Hz (Joris and Yin 1992). **C–F**, Simulated response of mouse low- (**C**, **D**) and high-SR fibers (**E**, **F**) to a 32-kHz tone (**C**, **E**) and 32-kHz SAM tone (**D**, **F**). *Depth of shading* indicates rate (**C**, **E**) and modulated rate (**D**, **F**) as indicated in the *scale* at the right.

99 dB SPL at 16 weeks (8 control, 10 exposed). Both histology and physiology were conducted 2 weeks after noise exposure.

Heterozygous breeding pairs of the mutant mouse line with targeted deletion of the gene for the alpha subunit of the BK_{Ca} channel were obtained from the laboratory of origin (Meredith et al. 2004). This same line has been used previously for studies on the role of the BK_{Ca} channel in the inner ear (Pyott et al. 2007; Maison et al. 2013a). The mice were maintained on an FVB/NJ background. Offspring of the heterozygous paternal stock were bred and genotyped in-house to produce homozygous null animals and wild-type littermates. Physiology was conducted at 6–8 weeks of age and included five control and five KO mice of mixed genders. The comparison here was between wild-type and KO mice; none of these mice were noise-exposed.

In one experiment, electrophysiology was conducted during application of ouabain to the round window niche in order to cause unilateral cochlear neuropathy (Lang et al. 2011; Yuan et al. 2014). After anesthetization, the pinna was removed and a retroauricular incision was made. The underlying muscles and facial nerve were separated by blunt dissection to expose the middle compartment of the bulla, and the round window niche was exposed through a small opening. Ouabain (1–2 µl, 1 mM in distilled water) was applied to the round window membrane for 20 min using a 10-µl Hamilton syringe, and then wicked off and exchanged for a fresh solution every 20 min for four total applications.

All procedures were approved by the Institutional Animal Care and Use Committee of the Massachusetts Eye and Ear Infirmary.

Physiology

Mice were anesthetized with ketamine (100 mg/kg i.p.) and xylazine (20 mg/kg i.p.). Recordings were conducted in an acoustically and electrically shielded room held at 30 °C. Custom LabVIEW and MATLAB software controlling National Instruments 24-bit digital input/output boards generated all stimuli and recorded all responses. Stimuli were presented using a custom acoustic assembly containing two electrostatic drivers (CUI CDMG15008-03A) and an electret condenser microphone (Knowles FG-23329-P07). The assembly was calibrated with a ¼-inch Bruel and Kjaer condenser microphone. All stimuli were presented unilaterally to the left ear, with the mouse on its right side, and the acoustic assembly just above the ear canal. In-ear calibrations were performed at the onset of each experiment.

DPOAEs were recorded in response to two tones f_1 and f_2, each presented to separate speakers to reduce system distortion (frequency ratio f_2/f_1=1.2, and level difference L_1=L_2+10 dB). DPOAE response was measured at $2f_1–f_2$ by Fourier analysis of the ear-canal sound pressure waveform. Stimulus duration was 1.6 s at each level combination (L_2 varied from 20 to 80 dB SPL in 5-dB steps). Threshold was defined as the interpolated f_2 level producing a DPOAE of 5 dB SPL.

Both ABR and EFR were recorded differentially with subdermal needle electrodes with the common ground at the base of the tail; four different electrode configurations were used (Fig. 2). The first two configurations were used after a dorsal-ventral incision at the intertragal notch of the ipsilateral pinna to allow direct visualization of the eardrum. Following the incision, electrode pairs were placed both (1) vertex (positive electrode) to ipsilateral pinna, with the latter just caudal to the intertragal notch and (2) contralateral pinna (positive) to ipsilateral pinna, with both electrodes caudal to the intertragal notch. This configuration pair was used for group 1. In group 1a, the pinna electrode was just caudal to the intertragal notch, which is the standard position used by our lab (vertex - $pinna_D$). In group 1b, the pinna electrode was placed slightly more ventral along the antitragus in order to increase the amplitude of early ABR waves (vertex – $pinna_V$). The second two configurations were used after removing the entire pinna and surrounding skin (8–10 mm posterior to the tympanic ring) to access the bulla and round

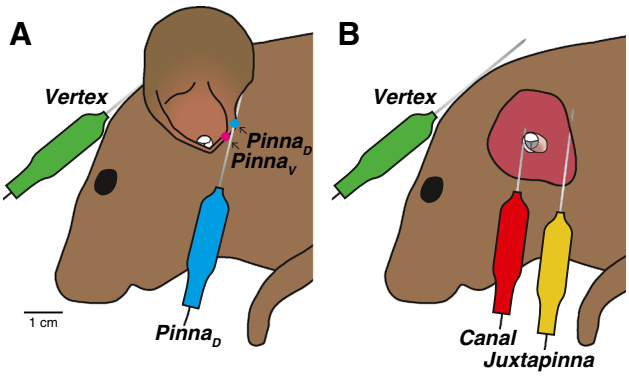

FIG. 2. Schematic of electrode configurations. **A** Intact-pinna configurations: vertex to $pinna_D$ shown, vertex to $pinna_V$ location illustrated by *magenta dot*. For pinna to pinna configurations, the positive (*green*) electrode was placed in an identical location on contralateral side (not shown). **B** Removed-pinna configurations: vertex to ear canal, vertex to juxta-pinnal skin.

window. Following that, electrodes were placed both (3) vertex (positive) to ipsilateral ear canal, with the latter through the rostral edge of the severed ear canal, and (4) vertex (positive) to ipsilateral juxta-pinnal skin, with the latter through the cut edge of the skin posterior to the ear canal. This configuration was used for group 2. Responses were measured simultaneously from each configuration pair.

Responses were amplified 10,000X using two Grass P511 amplifiers with a 0.3–3 kHz passband for ABR and a 0.03–30 kHz passband for EFR. ABRs were evoked with 5-ms tone-pips with 0.5 ms $\cos^2$ rise–fall presented in alternating polarity at a rate of 40/s. Tone-pip frequencies were 11.3 or 32 kHz. Trials where the response amplitude exceeded 15 μV were rejected; 512 artifact-free trials of each polarity were averaged to compute ABR waveforms. Threshold was defined by blinded visual inspection of the stacked waveforms as the lowest level at which a reproducible peak or trough appears, which usually occurs one-level step below that at which peak-to-peak amplitude begins to grow. EFR stimuli were 30 s. SAM tones using 100 % modulation depth and carrier frequencies (f_cs) of 11.3 or 32 kHz. Modulation frequency (f_m) ranged from 400 to 1990 Hz. EFR amplitude was measured at f_m using Fourier analysis. To minimize system distortion, the carrier tone was presented using one of the speakers and the two sidebands using the other. Post-mortem measurements demonstrated that this approach eliminated distortion for stimulus levels up to 90 dB SPL. In the mouse, the quadratic difference tone distortion product at f_m (generated by interaction of the carrier and either sideband) falls outside the range of

hearing for all f_ms used (up to 2 kHz), so it should not influence results. Cubic difference tones were measureable at f_c+nf_m for n={−4, −3, −2, +2}, but since their amplitude was always at least 50 dB lower than that of the stimulus tones, contribution to the EFR was minimal. EFR group delay was calculated for each individual by (1) measuring the phase at f_m by Fourier analysis, (2) unwrapping using MATLAB's *unwrap*, (3) fitting a line to each consecutive trio of points to find the local slope (group delay), and (4) smoothing with a three-point moving average. Modulation sampling was sufficiently fine (30- or 60-Hz steps) to unambiguously unwrap phase. EFR PLV (Dobie and Wilson 1989; Zhu et al. 2013) was calculated by (1) breaking the 30-s continuous record into 300 100-ms "trials" (Fig. 3A, top panel), (2) measuring the phase of each trial at f_m by Fourier analysis (Fig. 3B, thin lines), and (3) computing the magnitude of the vector average of all phases, assigning each vector equal amplitude (Fig. 3B, C, thick red line). "Trials" where voltage exceeded 15 μV were rejected as artifact. A trial length of 100 ms was chosen because it yielded a good signal-to-noise ratio for all data presented in this paper; for other datasets, a different length may be necessary. Under this protocol, PLV ranges from 0 (random phase) to 1 (each "trials" having identical phase).

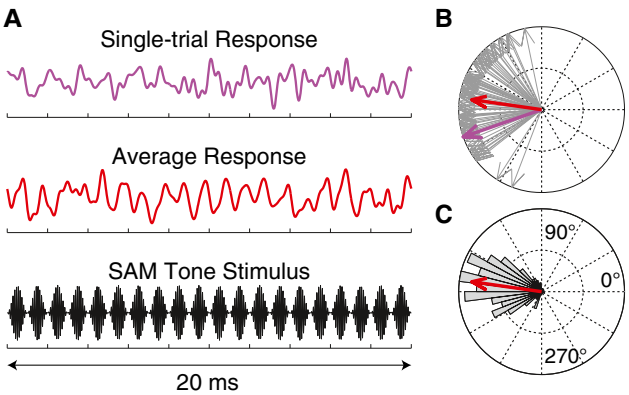

FIG. 3. EFRs were recorded in response to a 30-s. continuous SAM tone, a 20-ms sample of which is shown in **A**, along with a typical single-trial and average response. To compute EFR phase-locking value (PLV), the 30-s. response was split into 100-ms "trials" and the phase of each trial (**B**, *thin-line vectors*) was computed. The phase for the single trial in **A** is shown is color coded to match. For clarity, only 100 trials are shown in **B**; *Bars* in **C** show a histogram of all 300 trials. All 300 single-trial phases were vectorially summed to compute the PLV (**B** and **C**, *thick red line*).

Cochlear Immunostaining and Innervation Analysis

Mice were perfused transcardially with 4 % paraformaldehyde. Cochleas were decalcified, dissected into half-turns, and incubated in primary antibodies: (1) mouse (IgG1) anti-CtBP2 from BD Biosciences at 1:200 and (2) mouse (IgG2) anti-GluA2 from Millipore at 1:2000. Primary incubations were followed by 60-min incubations in species-appropriate secondary antibodies. Cochlear lengths were obtained for each case, and a cochlear frequency map computed using a custom ImageJ plug in (http://www.masseyeandear.org/research/otolaryngology/investigators/laboratories/eaton-peabody-laboratories/epl-histology-resources/) that translates cochlear position into frequency according to the published map for the mouse (Taberner and Liberman 2005; Müller et al. 2005). Confocal *z*-stacks from each ear were obtained using a glycerol-immersion objective (N.A.=1.4) and ×3.17 digital zoom on a Leica TCS SP5 confocal. Synapses in the IHC area were counted using Amira (Visage Imaging) to find the *xyz* coordinates of all the ribbons (CtBP2-positive puncta), and custom re-projection software was then used to assess the fraction of ribbons with closely apposed glutamate receptor patches (i.e., GluA2 puncta).

Statistical Analysis

Statistical testing was performed in MATLAB, using the *anova*, *ranova*, and *multicompare* functions for ANOVA, repeated-measures ANOVA, and post hoc tests. When statistically significant interactions were identified, post hoc two-sample *t* tests were performed using a Holm–Bonferroni correction for multiple comparisons.

RESULTS

Noise-induced Synaptic Loss after Reversible Noise-Induced Threshold Shift

We titrated the sound level of an octave-band noise (8–16 kHz) such that a 2-h exposure would produce a large temporary threshold shift (1 day post-exposure) but minimal permanent threshold shift (2 weeks post-exposure). For DPOAEs and ABRs, peak threshold shift at 24 h post-exposure was ~40–50 dB (data not shown). By 2 weeks post-exposure, DPOAE thresholds were not significantly elevated at any test frequencies except for at 45 kHz, where thresholds were elevated by 5–20 dB, depending on group (Fig. 4A). ABR thresholds, measured at 11.3 and 32 kHz, were not significantly elevated in any groups (Fig. 4B). Consistent with the observation that overall noise

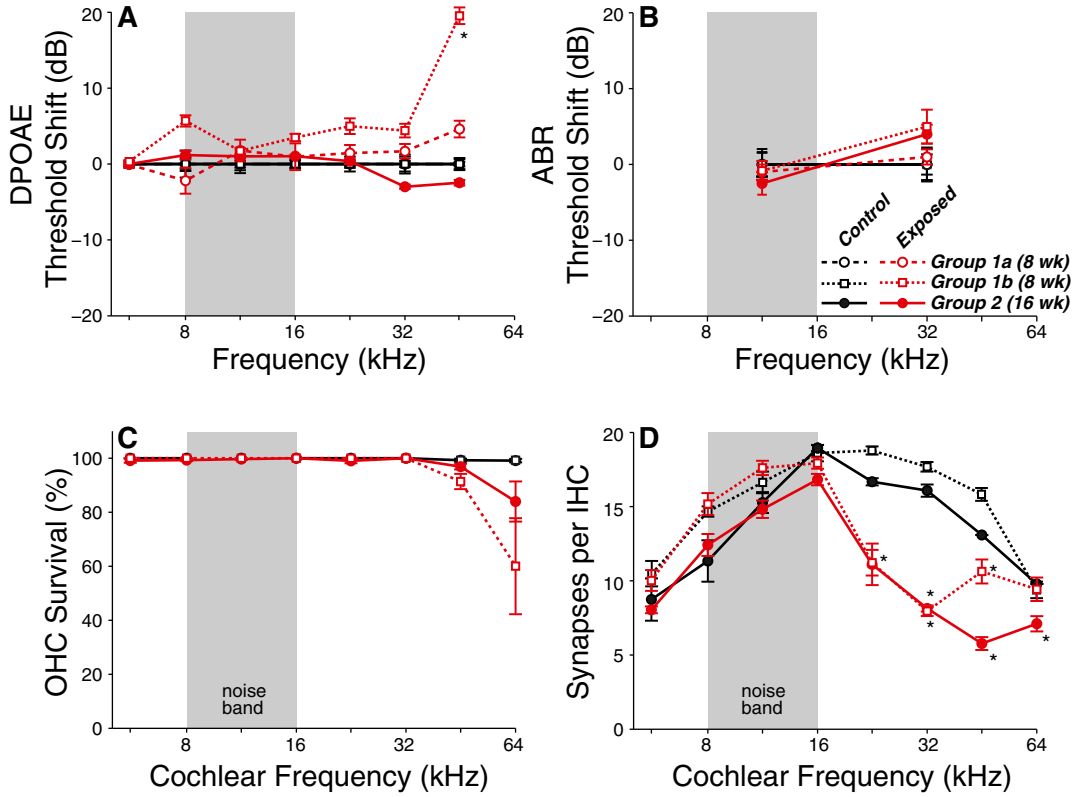

FIG. 4. Noise exposure causes permanent synaptic loss with minimal permanent threshold shift. Mean DPOAE thresholds (**A**) and ABR thresholds (**B**) for each of three different groups, normalized to their own age-matched controls: group 1a—exposed to 98 dB SPL at 8 weeks of age (4 control, 5 exposed); group 1b—exposed to 98 dB SPL at 8 weeks (6 control, 6 exposed); and group 2—exposed to 99 dB SPL at 16 weeks (8 control, 10 exposed). **C** OHC survival in control (*black*) and exposed (*red*) mice. **D**,Counts of pre-synaptic ribbons and post-synaptic glutamate receptors show loss of AN synapses on inner hair cells throughout the basal half of the cochlea. For histology (**C**, **D**), a subset of group 2 was used (three control, five exposed), all ears were used in groups 1a and 1b. **A** There were no significant effects of exposure on DPOAE thresholds by two-way repeated-measures ANOVA for groups 1a and 2: $F_{(1,42)}$=0.01 p=0.91 and $F_{(1,102)}$=0.05 p=0.83. For group 1b, the effect of exposure was significant (interaction between frequency and exposure condition $F_{(6,60)}$=5.97, p<0.001). **B** There were no significant effects of exposure on ABR thresholds: group 1a $F_{(1,7)}$=0.00, p=1; group 1b: $F_{(1,10)}$=1.24, p=0.29; group 2: $F_{(1,16)}$=0.33, p=0.57. **C** While the effect of exposure was significant (interaction $F_{(14,84)}$=3.07, p<0.01), there were no significant pairwise comparisons after Bonferroni–Holm correction. **D** There was a significant interaction between frequency and exposure group for both group 1b ($F_{(7,63)}$=16.56, p<0.001) and group 2 ($F_{(7,35)}$=8.26, p<0.001). *Stars* indicate significant paired differences (p<0.01 or better) between exposed and corresponding control.

vulnerability decreases with age from 8 to 16 weeks (Kujawa and Liberman 2006), complete threshold recovery was observed in the mice exposed at 16 weeks of age (Fig. 4A, B; group 2). The high-frequency threshold shifts in the 8-week exposure group were associated with scattered loss of OHCs in the extreme basal regions of the cochlea (Fig. 4C). While no significant differences were found in OHC loss between the animals exposed at 8 weeks and those exposed at 16 weeks, a trend towards more loss and a larger threshold shift suggest greater damage to OHC function in the 8-week group. There were no significant IHC losses in any ears (effect of exposure by two-factor repeated-measures ANOVA for groups 1b and 2: $F_{(1,63)}$=0.21 p=0.66 and $F_{(1,35)}$=0.01 p=0.94).

While noise exposure minimally affected cochlear thresholds, histological analysis clearly demonstrated loss of AN synapses (Fig. 4D). Each mammalian AN fiber contacts one IHC via a single synaptic terminal, with a single active zone, seen in the electron microscope as apposed pre- and post-synaptic plaques of membrane thickening, with a prominent pre-synaptic ribbon surrounded by a halo of synaptic vesicles (Liberman 1980; Stamataki et al. 2006). At the light-microscopic level, we can count the synapses between AN fibers and IHCs by immunostaining pre-synaptic ribbons and post-synaptic glutamate receptors using antibodies against a ribbon protein (CtBP2: Khimich et al. 2005) and an AMPA-type glutamate receptor subunit (GluR2: Matsubara et al. 1996). In control mice, the number of synapses per IHC varies with cochlear location, with a peak of ~18 synapses/IHC in the middle of the cochlear spiral (Fig. 4D). Noise exposure caused significant synaptic loss

throughout much of the basal half of the cochlea, with maximum losses occurring 1½ to 2 octaves above the noise-exposure band (Fig. 4D). At the 32-kHz region, the mean loss of synapses was 53 % (group 1b) and 50 % (group 2). Prior work has shown that this synaptic loss is permanent and followed by a delayed degeneration of spiral ganglion neurons (Kujawa and Liberman 2009).

EFR Measures in Noise-Exposed Ears: Effects of Modulation Frequency

EFRs were recorded 2 weeks after noise exposure in response to 30-s continuous SAM tones. We placed the carrier frequencies at 32 kHz (Fig. 5B, D, F, H) and 11.3 kHz (Fig. 5A, C, E, G) to probe cochlear regions with and without neuropathy, respectively (Fig. 4D). We varied modulation frequency from 400 to 1400 Hz to probe responses from different portions of the ascending auditory pathways. With ABRs, contributions from different auditory centers are, at least partially, separated in time (Melcher and Kiang 1996). With EFRs, responses from different nuclei are, at least partially, separated by modulation frequency: more peripheral neurons (e.g., AN) dominate at high modulation frequencies, whereas more rostral neurons (e.g., inferior colliculus) dominate at low modulation frequencies (Rickards and Clark 1972; Kuwada et al. 2002; Herdman et al. 2002). In exposed animals, EFR amplitudes were reduced by up to 55 % in response to the carrier frequency probing the neuropathic region (32 kHz), but unchanged for the non-neuropathic region (11.3 kHz). For the 32-kHz carrier, the maximum differences in amplitude were seen at higher modulation frequencies (near 1000 Hz), consistent with the idea that AN fibers contribute a larger portion of the response at these higher frequencies than more central auditory nuclei. We computed EFR PLV from the same data (see "Methods"). Changes in PLV mirrored the changes in EFR amplitude (Fig. 5C, D).

To better understand the generators of the EFR in mouse, we calculated group delay from the slope of the phase vs. modulation frequency function (Fig. 5E–H; see "Methods"). For a single generator, group delay is equivalent to the latency of that generator. Group delay becomes complicated when two sources contribute, but can still be informative near amplitude peaks, where group delay is equal to a weighted sum (by their amplitudes) of the two sources (Shera and Bergevin 2012). Consistent with traveling wave delays in the cochlea, 11.3-kHz carriers (Fig. 5G) gave rise to longer group delays than 32-kHz carriers (Fig. 5H) at the 1-kHz modulation frequency (arrows). The difference in group delays (3.1 vs. 2.0=1.1 ms) was significantly larger than that observed in ABR peak I latency (1.44 vs. 1.24=0.2 ms; two-sided paired t test $t_{(8)}$=3.44, p=0.009). The difference in first-spike latency of mouse AN fibers at these two CF regions is intermediate (3.0 vs. 2.5=0.5 ms; Figs. 4 and 5 of Taberner 2005). EFR group delay was unchanged following noise exposure except at amplitude minima (Fig. 5G, H), suggesting little shift in the locus of the neuronal groups dominating the responses. Large swings in group delay near amplitude minima do not necessarily indicate a change in generators, as phase vs. frequency gradients can be complicated when multiple sources destructively interfere (see "Discussion").

Effects of Electrode Placement on EFR Measures: Determining Sources

The EFRs in Figure 5 were recorded with a vertex to pinna electrode configuration (see "Methods"), similar to that used in clinical settings (Hall 2006: 201–207). However, noise-induced cochlear neuropathy may be more robustly detected by electrode configurations that increase the relative contributions from peripheral generators, such as electrodes on the tympanic membrane or round window niche as used in electrocochleography (Schwaber and Hall 1990). To mimic these configurations in the mouse, we removed the pinna and placed the negative electrode through the cartilage of the ear canal, leaving the positive electrode at the vertex see Fig. 2B. This increased the amplitude of wave I and revealed a short-latency shoulder on wave I (Fig. 6A), which is the analog of the summating potential (SP) recorded on the round window, reflecting summed receptor potentials from IHCs (Durrant et al. 1998; Yuan et al. 2014). Contributions of IHCs and AN fibers were also increased in the EFRs, as group delays around 1 kHz (the amplitude peak) were shorter than those measured with the vertex to pinna configuration (Fig. 6C, black vs. gray line). Due to destructive interference between multiple sources, large group delay excursions around amplitude minima are not close to the latency of either source. Therefore, the large reversal of group delays around 750 Hz does not indicate a sudden change in the source of the EFRs at this frequency.

To validate the use of group delay to infer EFR generators, we made measurements in one mouse before and after inactivating AN responses, without affecting hair cell function, by round window application of ouabain, a blocker of a neural-specific Na/K ATPase (Azarias et al. 2013; Obrien et al. 1994; Schmiedt et al. 2002). Ouabain effectively eliminated all ABR waves except those from pre-synaptic sources, i.e., the SP (Fig. 6A, green line). Both EFR functions flattened, consistent with a transformation from

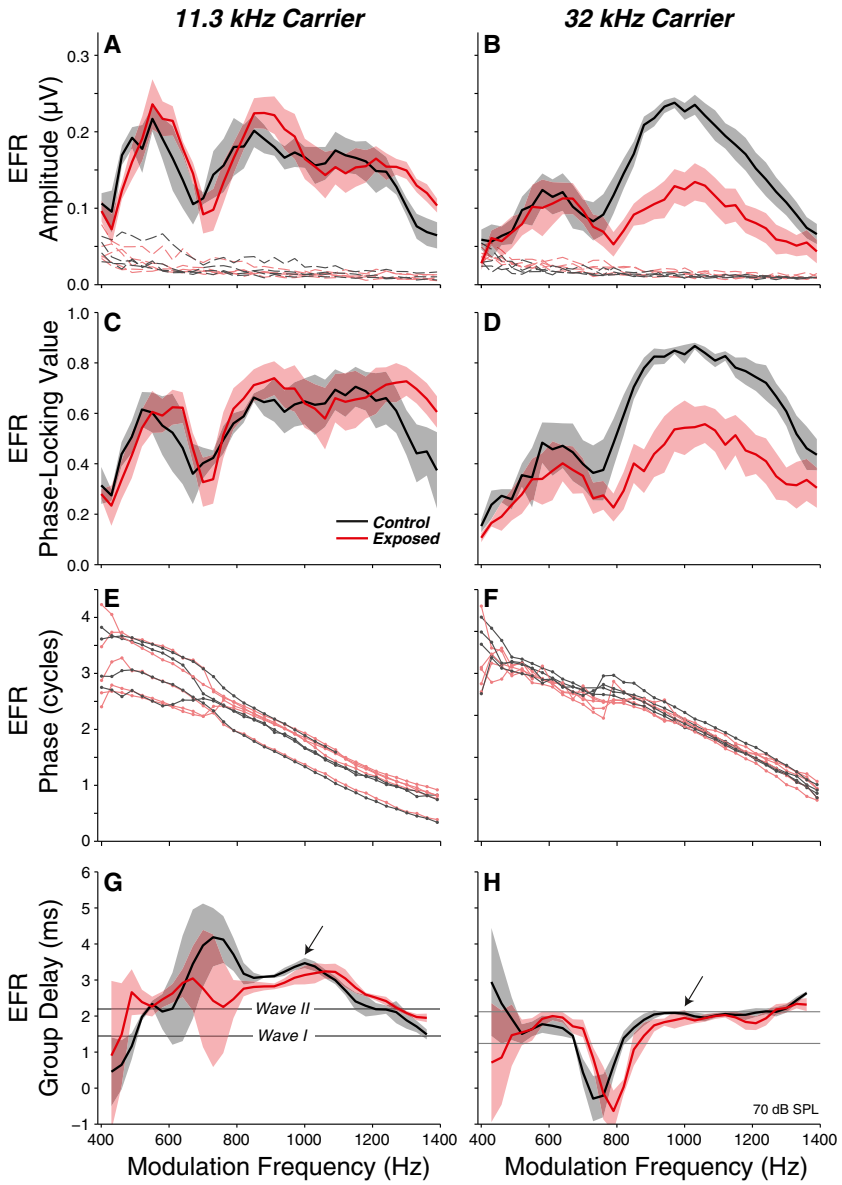

FIG. 5. Cochlear neuropathy reduces EFR amplitudes and phase-locking values (PLVs). **A**–**D** EFR amplitude (**A**, **B**) and EFR PLV (**C**, **D**) were decreased in the noise-exposed group for 32-kHz carriers (**B**, **D** $F_{(1,231)}$=6.21, p=0.041; $F_{(1,231)}$=5.75, p=0.048), but not for 11.3-kHz carriers (**A**, **C** $F_{(1,231)}$=0.32, p=0.59; $F_{(1,231)}$=0.18, p=0.68). **E**, **F** EFR phase, unwrapped for each individual and shifted by an integer number of cycles for best alignment in the 1 to 1.4 kHz range. **G**, **H** EFR group delays, computed as the slope of phase vs. modulation frequency functions on an individual basis (see "Methods"). *Horizontal lines* show ABR peak latencies measured at 70 dB SPL, the same level used for the SAM tone response shown here. *Thin dashed lines* show individual noise floors (**A** and **B** only), *thin solid lines* show individual responses (**E** and **F**), and *thick lines* and *shaded areas* show group means±SEMs. Data are from group 1a, recorded using the vertex to pinna$_D$ electrode configuration.

multiple interacting sources to a single, short-latency source (Fig. 6B, C). Since EFR group delay was approximately equal to SP latency (0.8 ms), the post-ouabain EFR is likely generated by the IHCs: the SAM tone is similar to a series of rapid tone bursts, in response to which IHC receptor potentials fluctuate at the envelope frequency.

To determine if the vertex to ear canal configuration provides a more robust indicator of cochlear neuropathy, we measured ABRs and EFRs from two electrode configurations in one group of control and noise-exposed ears after completely removing the pinna: (1) vertex to cartilaginous ear canal (Fig. 7C, I, O) vs. (2) vertex to juxta-pinnal skin (Fig. 7D, J, P; see "Methods"). EFR amplitudes were reduced by neuropathy for both configurations, but dependence on modulation frequency was more complex in the vertex to ear canal configuration, suggesting greater constructive and destructive interference among multiple generators. At 1330 Hz modulation, the locus of

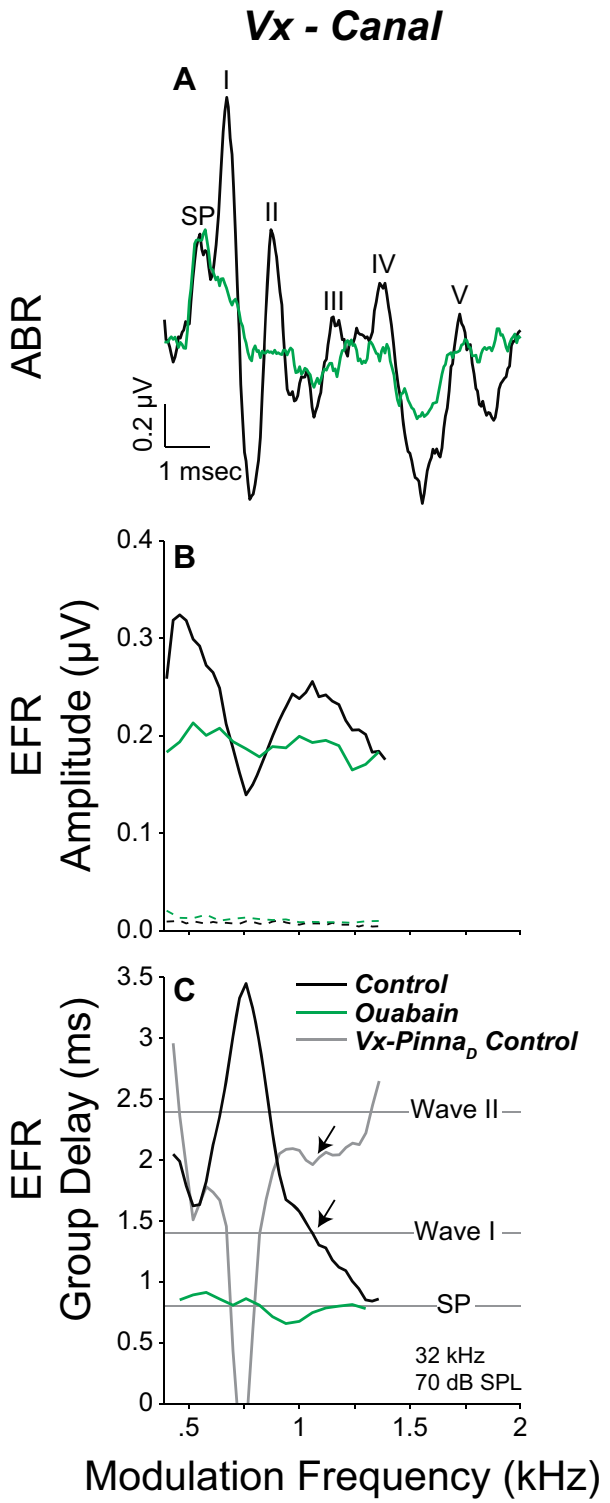

FIG. 6. Acute ouabain-induced neuropathy reveals hair cell contributions to ABRs and EFRs. **A** ABR waveforms in response to 70-dB SPL, 32-kHz tone-pips. **B**, **C** EFR amplitude and group delay in response to a 32-kHz carrier at 70 dB SPL. *Horizontal lines* in **C** show ABR peak latencies. In all panels, responses are shown before (*black*) and after (*green*) cochlear neuropathy induced by ouabain application to the round window. Data are obtained using the vertex to ear canal electrode configuration in an 8-week-old mouse. *Gray line* in panel **C** replots control vertex to pinna$_D$ mean group delay from Fig. 5H.

the amplitude peak for the vertex to ear canal configuration, group delay was significantly shorter than for the vertex to juxta-pinnal configuration (Fig. 7O vs. P), suggesting a greater contribution from peripheral generators, as confirmed by the relative heights of the early ABR waves (Fig. 7C vs. D). At the highest modulation frequencies, group delays for both configurations fell below 1 ms, indicating that responses were dominated by hair cell potentials.

As a fourth electrode configuration, we measured from ipsilateral pinna to contralateral pinna, thinking that this symmetrical placement ought to emphasize AN and cochlear nucleus contributions over those from higher auditory centers such as the inferior colliculus, given that the peripheral structures are more asymmetrically located with respect to the two electrodes (Ping et al. 2007). In two series of exposed and control ears, responses were simultaneously recorded from vertex to pinna (Fig. 7A, E, K, B, G, M) and pinna to pinna (Fig. 7F, L, H, N). Group delays were not generally shorter for the pinna to pinna configuration, perhaps because even the lowest modulation frequencies tested may still be too high for colliculus neurons, which respond poorly when modulation frequencies exceed 400 Hz (Fig. 9 of Joris et al. 2004).

In group 1b the pinna electrode was placed slightly more ventral along the antitragus. Perhaps because this decreased the distance to the cochlea, this configuration resulted in a significantly larger SP and wave I amplitude with respect to group 1a (Fig. 7A vs. B). Along with this small change in ABR, we observed increased EFR amplitudes and shorter group delays at low modulation frequencies (Fig. 7E, K vs. G, M), consistent with EFR contributions from AN responses throughout the modulation frequency range tested.

To more directly assess the effects of electrode configuration and modulation frequency on the detection of cochlear neuropathy, we computed amplitude ratios for responses measured in exposed vs. control ears. As shown in Fig. 8C, amplitudes were reduced over a broad range of modulation frequencies in most electrode configurations. Surprisingly, although the vertex to ear canal configuration showed the largest AN contributions (as seen in the ABR), this configuration was the least effective in yielding consistent EFR amplitude reductions over a wide range of modulation frequencies (Fig. 8C, purple line). Since the ability to separate two groups depends not only on the means, but also their variability, we

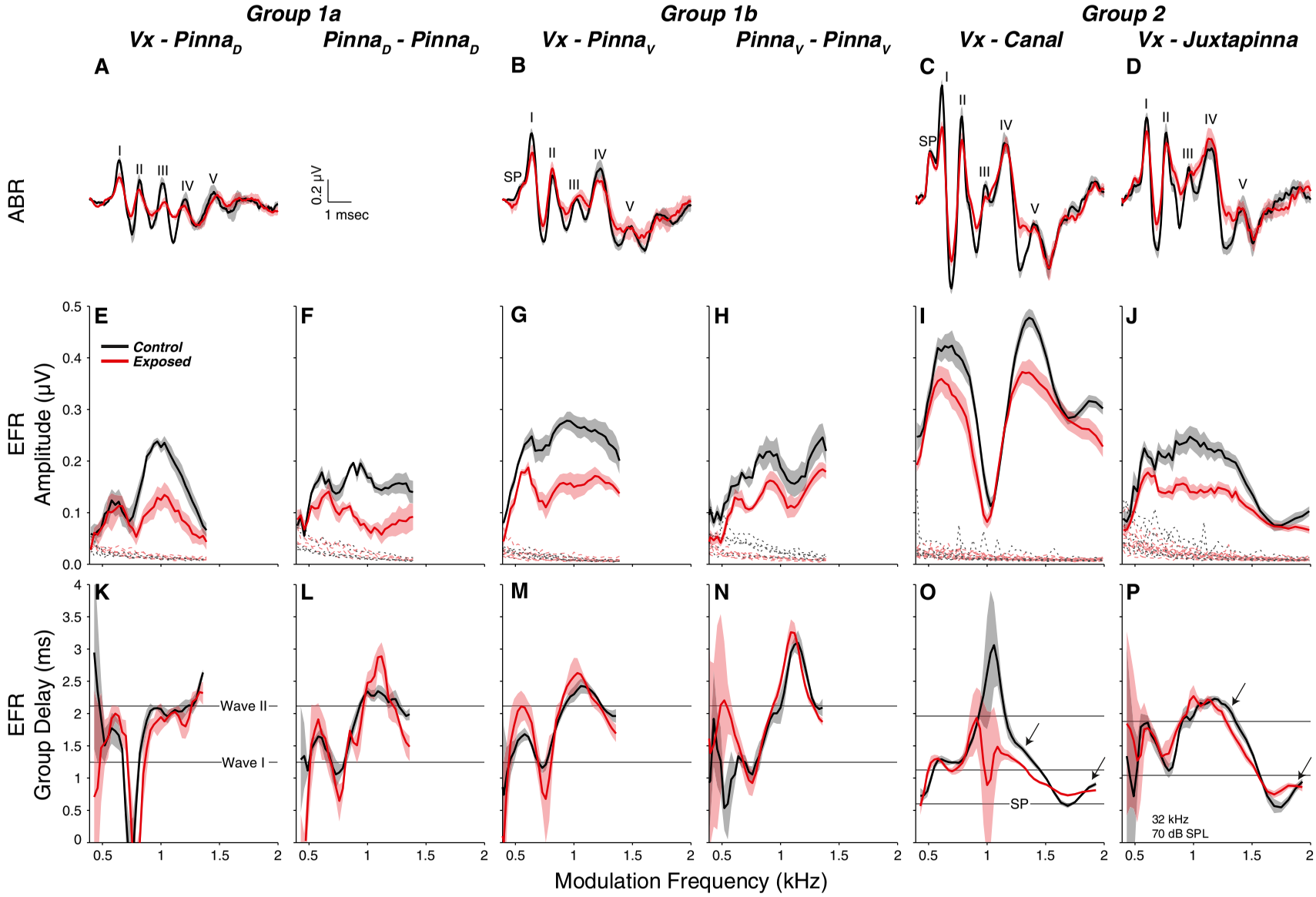

FIG. 7. Effects of electrode configuration on EFRs and ABRs. **A–D** Mean ABR waveforms in response to 70-dB SPL, 32-kHz tone-pips. **E–J**, Mean EFR amplitudes and **K–P** mean group delays in response to 32-kHz carriers at 70 dB SPL. *Horizontal lines* (**K–P**) show ABR peak latencies; SP latency is shown only when a clear local maxima is found. Because ABRs were not recorded for the pinna to pinna configuration, latencies (**L**, **N**) are from vertex to pinna data. *Thin dashed lines* (**E–J**) show individual noise floors. *Thick lines* and *shaded* areas in all panels show group means±SEMs. Wave I amplitude was significantly increased by a slight change in the location of the pinna electrode (**A** vs. **B**; two-way repeated-measures ANOVA: $F_{(1,17)}$=10.17, p=0.005). For group 2, group delay was significantly affected by electrode configuration (**O** vs. **P**; three-way repeated-measures ANOVA: $F_{(1,231)}$=6.20, p=0.02, significant pairwise effect of electrode configuration at 1330 Hz (*arrows*), p=0.002).

calculated effect size (Hedge's g), the difference in means divided by the pooled standard deviation (Hentschke and Stüttgen 2011). As shown in Fig. 8A, effect size exceeded one standard deviation over a broad frequency range for the vertex to pinna, pinna to pinna, and vertex to juxta-pinnal configurations, but not for the vertex to ear canal configuration (orange vs. purple lines). With EFRs, detection of neuropathy using an electrode configuration more sensitive to cochlear sources may be detrimental, as AN reductions due to neuropathy are diluted by hair cell potentials, which are unchanged. For such configurations, choice of modulation frequency becomes critical.

Ratio and effect size computed from PLVs were similar to those of amplitude, but effect size reached lower maximum values (Fig. 8B, D). In cases where signal-to-noise ratio (SNR) was very high (Vx-Canal, see Fig. 7I), PLVs became saturated and were therefore less useful for detecting neuropathy (Fig. 8B, D; purple line). In the pinna to pinna configuration of group 1b, noise floors were higher in some control animals (Fig. 7H). This caused the two groups to have similar SNRs, and thus PLVs, so effect size was small (Fig. 8D, filled triangles). PLVs appear not to be useful in high-SNR conditions such as these, but may be helpful in situations where SNR is poor.

EFR amplitude reductions were minimal at low modulation frequencies (below ~600 Hz) for all configurations and groups (Fig. 8C). If EFR at high modulation frequencies is dominated by more peripheral sources (i.e., hair cells and AN fibers), and by more central sources (e.g., inferior colliculus) at lower modulation frequencies (Kuwada et al. 2002), these data could be reflecting an amplified central auditory response in the face of peripheral response reductions after trauma (Gu et al. 2012; Schaette 2014). This speculation is supported by the ABR data (Fig. 9): while noise exposure significantly decreased the amplitudes of waves I, II, and III, waves IV and V were unaffected. Data in Figure 9 are for the vertex to pinna configuration of group 1a. For group 2, waves III and V were too small to measure in individual cases, but the trend towards less reduction in later waves can be seen in the mean waveforms: wave I ratios 0.66 and 0.70 vs. wave IV/V ratios 0.98 and 1.08 for Figure 7C, D, respectively. However, waves I and IV/V were equally reduced in group 1b (0.68 vs. 0.69; Fig. 7B). This difference could be due to the mild threshold shift observed in that group (Fig. 4A).

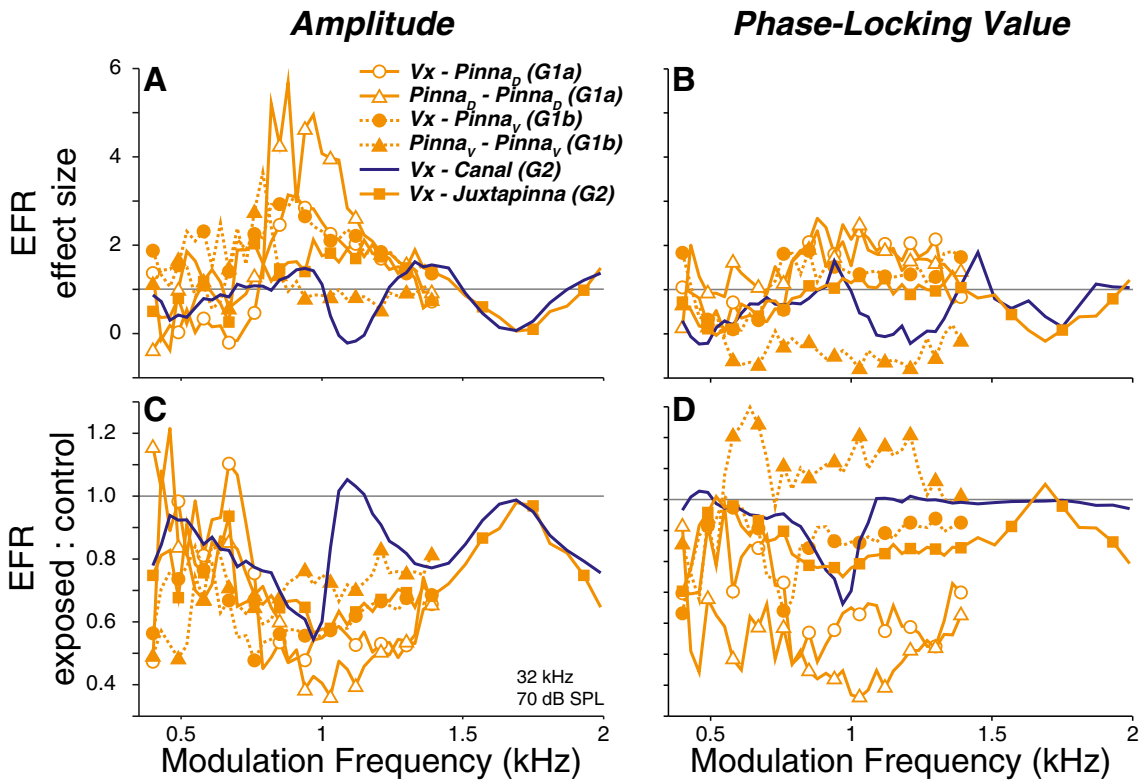

FIG. 8. EFR amplitudes (**A**, **C**) and phase-locking values (**B**, **D**) are most sensitive to cochlear neuropathy for modulation frequencies near 1 kHz. **A**, **B** The effect size (Hedge's g; Hentschke and Stüttgen 2011) is the difference in group means (control vs. exposed) divided by the square root of the weighted sum of group variances. Higher values indicate greater separation of the two groups. **C**, **D** Ratio between control and exposed means. Data in all panels are for the 32-kHz carrier at 70 dB SPL. Key in **A** applies to all panels.

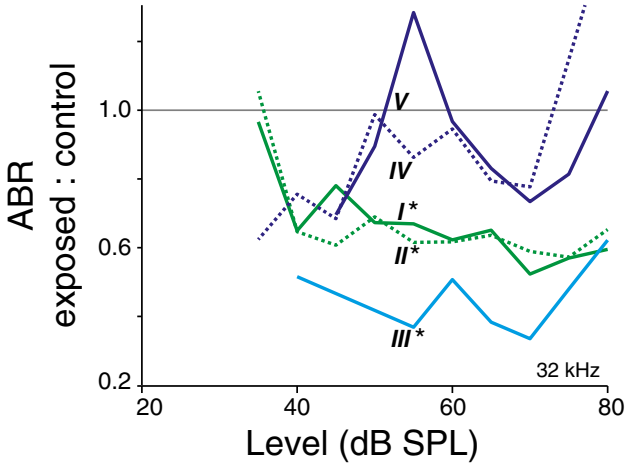

FIG. 9. Amplitude ratios between control and noise-exposed groups for each of the five ABR waves suggest central compensation. ABR waves were identified using a derivative-based peak-finding algorithm, and are measured peak-to-trough. Data are from group 1a, recorded using the vertex to pinna$_D$ electrode configuration. There was a significant interaction between wave and exposure by a three-way repeated-measures ANOVA: $F_{(4,35)}$=3.19, p=0.025. Significant exposed/control differences for each wave are indicated by *stars*: [I, II, III, IV, V], p=[0.004, 0.015, 0.002, 1, 1].

EFR Measures in Noise-Exposed Ears: Effects of Stimulus Level

We recorded amplitude vs. level functions for ABR and EFR at a variety of modulation frequencies for all three groups of noise-exposed mice. For brevity, only responses from the vertex to pinna configuration (group 1a) are shown in Fig. 10, but they are representative of all three groups. ABR wave I (Fig. 10A, B) showed the behavior expected based on prior studies of noise-induced neuropathy in mice (Kujawa and Liberman 2009), i.e., a fractional reduction of response amplitudes at 80 dB SPL comparable to the fractional loss of synapses in the appropriate cochlear region.

To examine the level dependence of noise-induced changes in EFR, we used the modulation frequency producing the largest responses in controls: 820 Hz for the 11.3-kHz carrier and 1000 Hz for the 32-kHz carrier (Fig. 5A, B). The EFR data (Fig. 10C, D) showed the same trends as seen in the ABR; however, the noise-induced changes in EFR were more robust: the scatter was smaller, and the inter-group difference were clearer. Changes to EFR PLV were similar to changes in EFR amplitude. This phase-locking measure may be particularly useful when signal-to-noise is poor (Zhu et al. 2013).

To more quantitatively assess the separability of control vs. noise-exposed groups in EFRs and ABRs, we calculated amplitude ratio and effect size as a function of level (Fig. 11). Several general trends are seen regardless of electrode configuration. First, as suggested from the mean data, the effect sizes are higher with EFRs than with ABRs at all but the highest sound pressure levels, where EFRs become less affected by neuropathy, while effects on ABRs increase (Fig. 11A–F). This tendency likely reflects the fact that AN synchrony to amplitude-modulated tones rises with sound pressure level to a peak and then falls, whereas rate response to pure tones rises to saturation and does not decline with further level increases.

The second general trend emerging from the effect size and ratio data (Fig. 11) is that effects of neuropathy are minimal on both ABR and EFR at low sound levels. This trend is consistent with the idea that the noise damage is selective for fibers with low SRs and higher thresholds (Furman et al. 2013): since they do not normally contribute to either EFRs or ABRs at near-threshold levels, their loss does not affect the amplitudes of either.

Thirdly, it is important to consider the effects of modulation frequency. Across all electrode configurations, the most robust inter-group differences were seen with modulation frequencies between 820 and 1330 Hz. Using a higher modulation frequency, e.g., 1810 Hz, was less robust in detecting neuropathy, presumably because at such a high frequency, the hair cell contributions begin to dominate the responses. EFRs were also less useful at low modulation frequencies, e.g., 550 Hz (Fig. 11A, B, G, H), perhaps due to a larger contribution from more central generators, less affected by neuropathy due to central compensation (Fig. 9).

Lastly, choice of electrode configuration also affected the maximum effect size. Separation was best for the group 1a pinna to pinna configuration (Fig. 11B), despite a lack of AN dominance evidenced in the group delays (Fig. 7M). Effect sizes were not as high in group 1b (Fig. 11D), suggesting that small differences in electrode location can strongly affect the results (see also Fig. 7F vs. H). The electrode configuration chosen to maximize contributions from the AN (vertex to ear canal) did not produce maximal effect sizes (Fig. 11E), although response amplitudes were increased (Fig. 7I). This presumably reflects the fact that the proximity of the ear canal to the cochlea increases the size of the hair cell contributions as well as the AN contributions. These sources are separable in ABRs, so the increased AN signal increases effect size. Since they are mixed in EFRs, hair cell potentials decrease effect size since they are not altered by the neuropathy.

There were no differences in mean SP amplitude between control and neuropathic groups, indicating no hair cell dysfunction (see waveforms in Fig. 7C). Intra-subject variability in ABR amplitudes caused by slight differences in anatomy or electrode placement might affect SP and wave I equally. Therefore, we

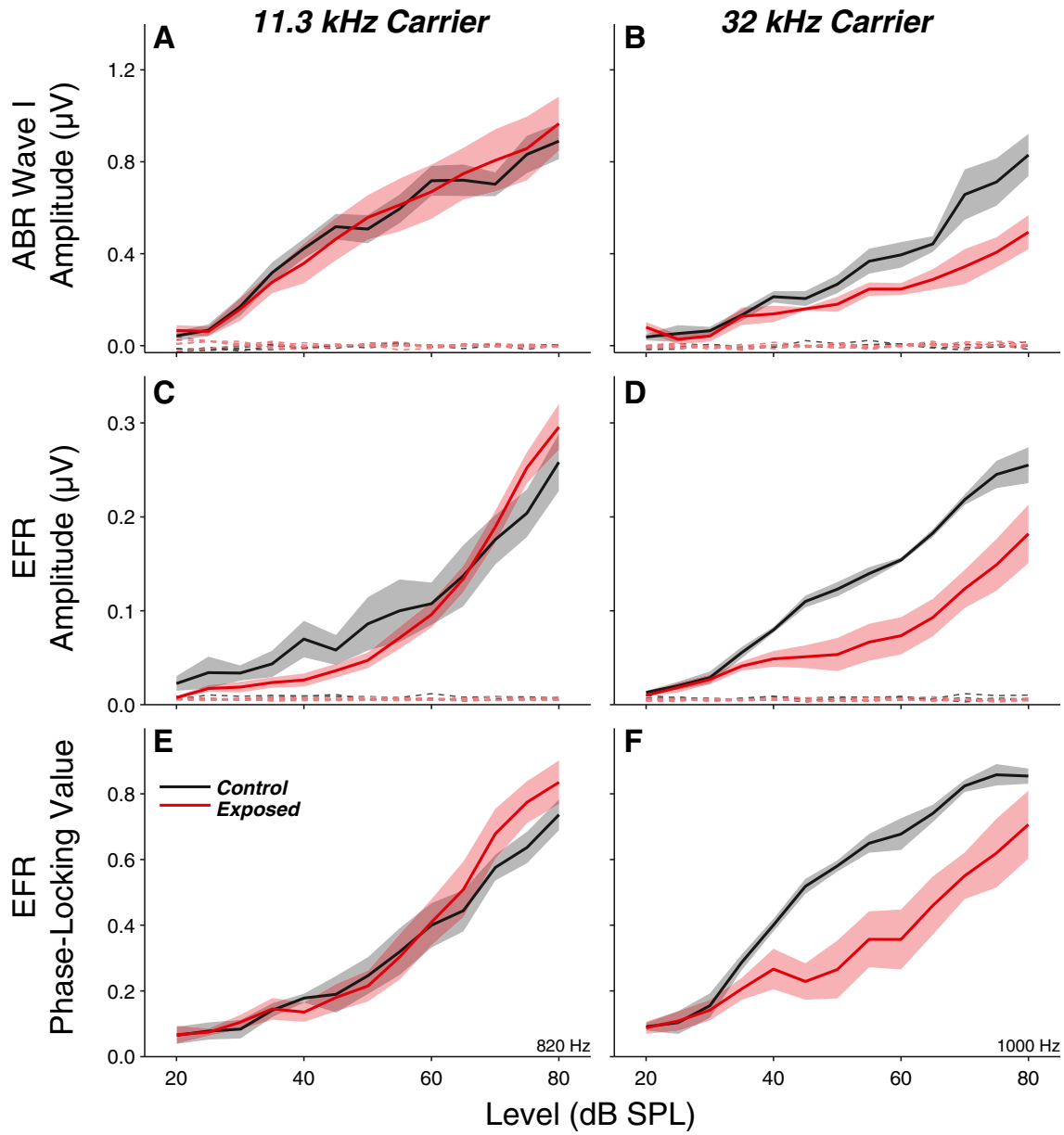

FIG. 10. After neuropathic noise, changes in EFR amplitude (**C**, **D**) and phase-locking values (**E**, **F**) were more robust than changes in ABR Wave I amplitude (**A**, **B**). EFR data were measured at the modulation frequency producing the largest response in normal mice: 820 Hz for the 11.3-kHz carrier and 1000 Hz for the 32-kHz carrier (see Fig. 4). ABR wave I amplitude was measured peak to following trough. *Thin dashed lines* show individual noise floors, and *thick lines* and *shaded areas* show group means±SEMs. Data are from group 1a, recorded using the vertex to pinna$_D$ electrode configuration.

wondered if normalizing wave I amplitude by SP in each case could improve the ability to detect neuropathy. However, effect sizes calculated from the wave I/SP ratio were lower than those for wave I alone (Fig. 11E, downward- vs. upward-pointing triangles). Analysis of the individual waveforms revealed that SP and wave I amplitudes were not correlated within each group (data not shown).

In one of our noise-exposed groups, neuropathy was accompanied by high-frequency threshold shift and OHC loss at the basal end of the cochlea (Fig. 4, group 1b). Since clinical cases with OHC damage superimposed on cochlear neuropathy are likely to be common, it is useful to compare it with cases of pure neuropathy. Unlike in group 1a (Fig. 11G), amplitudes in exposed ears were reduced even at low SPLs (Fig. 11I). If this reduction were due to a substantial loss of both low- and *high*-SR fibers, ratios would further decrease as SPL increases to moderate levels due to the decreased low-SR contribution. Since ratios do not decrease, EFR changes are likely the result of a combination of hair cell dysfunction and low-SR fiber

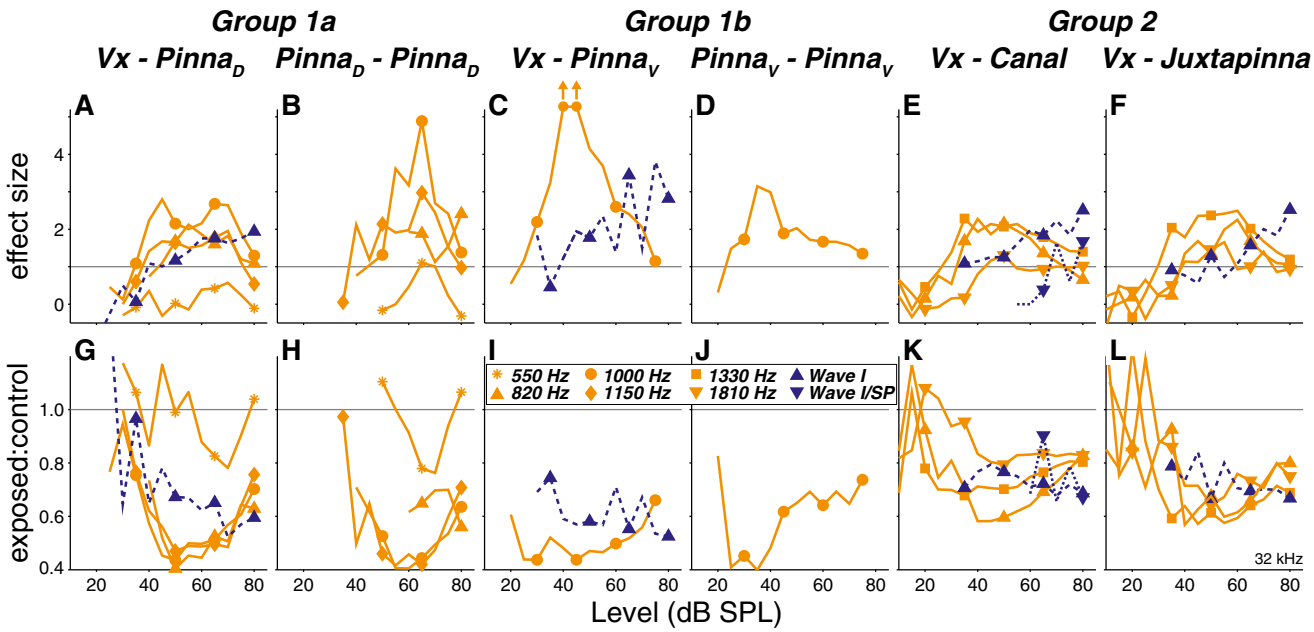

FIG. 11. EFR is a more powerful measure of cochlear neuropathy than ABR, and effect sizes are largest at moderate SPLs. **A–F**, Effect sizes (Hedge's g) for pairwise comparison between each noise-exposed group and its respective controls for both ABR (*purple*) and EFR (*orange*) measures. **G–L**, Simple ratios for the same pairwise comparisons shown in **A–F**. For clarity, only levels at which mean responses were one standard deviation above the mean noise floor are displayed. Key applies to all panels. *Upward arrows* in **C** show that the effect sizes were off scale: 7.01 and 7.03 at 40 and 45 dB SPL, respectively.

loss. Due to low inter-subject variability, EFR effect size was very high, peaking to 7.0 at 45 dB SPL (Fig. 11C).

EFR and ABR variability due to anatomical variation might be minimized by within-subject normalization. In humans, correlations between EFR amplitude and psychophysical performance are improved by using the slope of the EFR amplitude vs. modulation depth function (Bharadwaj et al. 2015). Transforming the data in Fig. 11 into slope vs. level functions significantly improved (decreased) exposed/control ratios (mean 0.45, $t_{(20)}$=3.17, p=0.005), but did not significantly enhance effect sizes (two-sided paired t test, $t_{(20)}$=1.05, p=0.31). Normalization may have been ineffective because anatomical variation in genetically identical mice is smaller than in humans, and therefore may not be a substantial source of variability.

For all groups and electrode configurations, neuropathic effects on EFR amplitude decrease at high levels, while effects on ABR increase (Fig. 11, bottom). This is likely due to differences in AN responses to SAM tones vs. tone-pips. Whereas responses to tone-pips saturate at 10 to 20 dB above threshold, modulated rate to SAM tones peaks around 30 dB above threshold, then decreases with increasing level (Fig. 1A vs. B). Thus, as sound level increases, the proportion of the EFR generated by fibers with CFs at the carrier frequency decreases (Fig. 1D, F). Above the low-SR modulated rate peak (~50 dB SPL, vertical dashed blue line), basal spread of excitation causes the high-SR contribution to increase, and the impact of low-SR loss is reduced. Since the low-SR response to tone-pips does not decrease at high levels, the impact of low-SR loss on the ABR increases at high levels (Fig. 1C, E). Furthermore, the neuropathy at the base of the cochlea (64 kHz) is less pronounced than at the carrier frequency (32 kHz; Fig. 4D), thus the overemphasis of EFRs on off-CF contributions further reduces its detection power at high levels.

EFR Measures in BK Knockout Ears

We compared low-SR specific noise-induced neuropathy with a model affecting all SR groups equally: mice with targeted deletion of the large-conductance, Ca^{2+}-activated K^+ channel (BK). These KO mice show lower sound-evoked discharge rates, for all SR groups, without any significant alterations in OHC function, as demonstrated by normal DPOAEs (Oliver et al. 2006). As seen in the control CBA/CaJ mice used in the noise experiments, the FVB/NJ control mice from the BK KO strain show amplitude vs. modulation frequency functions with two broad peaks, one at ~500 Hz and a second at ~1000 Hz (Fig. 12). In the KO mice, as expected, EFR amplitude (Fig. 12A, B) and PLV (data not shown) were significantly reduced at both 11.3- and 32-kHz carrier frequencies. Furthermore, the BK deletion caused an EFR reduction across all tested

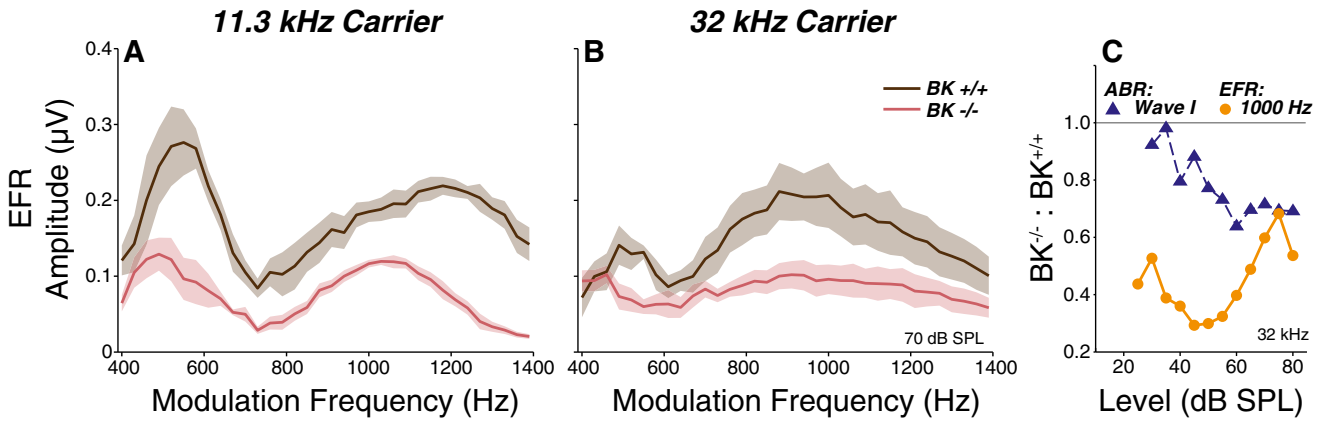

FIG. 12. BK channel knockout decreases EFR amplitudes over a wide range of carrier frequencies, modulation frequencies, and levels. **A**, **B** Mean EFR amplitudes (±SEMs) for 11.3-kHz (**A**) and 32-kHz carriers (**B**) at 70 dB SPL in BK knockout mice ($BK^{-/-}$) and wild-type controls ($BK^{+/+}$). There was a main effect of exposure by three-way repeated-measures ANOVA: $F_{(1,16)}$=27.1, p<0.001 and significant paired effects at both 11.3 (p<0.001) and 32 kHz (p=0.011). **C** Mean EFR amplitude ratios as a function of stimulus level for the 32-kHz carrier at 1-kHz modulation. All responses were measured using the vertex to $pinna_D$ electrode configuration.

modulation frequencies, perhaps because the BK channel is also expressed in neurons throughout the central auditory pathways (Sausbier et al. 2006).

We measured EFR amplitude vs. level functions at the same modulation frequencies used in the noise experiments (820 for 11.3 kHz and 1000 Hz for 32 kHz). EFR amplitude and PLV (not shown) were both reduced as in noise-induced neuropathy. However, in contrast to the results seen after noise, the response reduction in the BK KO mice occurred even at stimulus levels just above threshold (Fig. 12C). Reductions continued to increase up to 50 dB SPL, consistent with a deficit in all SR groups without any hair cell dysfunction (contrast with Fig. 11I, where reductions are present at threshold, but do not increase with level). While EFR amplitude reductions were greater than in noise-exposed mice, ABR wave I amplitude reductions were smaller. There are three possible reasons for this difference: (1) BK deletion causes a larger decrease in AN steady-state rate than in onset rate (Oliver et al. 2006), (2) although IHC time constants are increased in BK KOs, many AN fibers have normal onset rates and first-spike latencies (Oliver et al. 2006), and (3) unlike ABR wave I, the EFR contains contributions from central auditory neurons, which likely also express BK.

DISCUSSION

Contributions of Low- vs. High-SR Fibers to ABR vs. EFR: Insight from Single-Fiber Studies

Single-fiber recordings suggest that the noise-induced cochlear neuropathy observed in the present study is selective for the subset of AN fibers with low SR and high threshold (Furman et al. 2013). By "low SR," we mean the fiber groups initially characterized in cat as "low" and "medium" SR, i.e., the low-rate peak of the bimodal distribution of SRs, which includes ~40 % of the AN population. Although neuropathy was detected by both ABR and EFR, the changes in EFRs were more robust (Fig. 11). The differences between the tests can be understood based on known differences in the responses of high- vs. low-SR fibers to the different stimuli used to generate these auditory evoked potentials; i.e., short tone bursts for ABR vs. continuous amplitude-modulated tones for EFR.

As schematized in Fig. 1A, the ratio of peak to steady-state rate is higher in high-SR fibers than low-SR fibers (~3.5 vs. ~2.5 in mice, Taberner and Liberman 2005). Since the ABR is dominated by onset responses, the contribution of low-SR fibers to ABR wave I is smaller than their relative numbers (~40 % of the population) would predict. Recordings after selective damage by ouabain administration indicate that fibers with the lowest SRs (<1 sp/s) contribute little to ABR wave I amplitude (Bourien et al. 2014).

A second important factor is the SR-related difference in response synchrony (Fig. 1B). AN responses to amplitude-modulated tones can be quantified in terms of their average rate and synchronization index, i.e., the extent to which spikes are phase-locked to a periodic stimulus (Joris and Yin 1992; Cooper et al. 1993). Although the maximum modulated rate (the amplitude of the period histogram at the modulation frequency) of low-SR fibers can be lower than their high-SR counterparts, the maximum synchronization index (0.5*modulated rate/average rate) is typically higher, because there are fewer spontaneous (and therefore non-stimulus-locked) spikes in the response. Theoretically, EFR amplitude is proportional to the modulated rate of contributing neurons. Thus, when

average rates are comparable (i.e., at moderate-to-high levels), the enhanced synchrony of the low-SR fibers makes their EFR contribution larger than their relative numbers would predict.

Low-SR thresholds to pure tones and SAM tones are 10–20 dB higher than for their high-SR counterparts (Joris and Yin 1992; Fig. 1B). Therefore, loss of low-SR fibers should affect neither ABR nor EFR amplitudes until stimulus levels exceed ~30 dB SPL. This prediction is confirmed by the amplitude ratios between normal and neuropathic mice plotted vs. stimulus level (Fig. 11, *bottom*). However, it seems that even a small amount of threshold shift causes amplitude reduction at low stimulus levels, masking the low-SR specificity of the neuropathy (Fig. 4A, group 1b). Correspondingly, EFR reduction is visible in BK KO mice even at the lowest stimulus levels (Fig. 12), consistent with impairment in responses from all SR types (Oliver et al. 2006). A detailed model incorporating a continuous distribution of SR and CF would be able to incorporate EFR changes across multiple stimulus conditions, perhaps revealing more sensitive techniques to pinpoint the etiology of sensorineural hearing loss.

Generators of the EFR

Neurons throughout the auditory pathway can follow the envelope of amplitude-modulated sounds and therefore can theoretically contribute to the EFR (Kuwada et al. 2002). Unlike ABRs, the different cellular generators of EFRs are not separable in the time-domain response. However, evidence suggests that different generators dominate the response at different modulation frequencies. The high-frequency limit of phase-locking to modulation frequency decreases as the signal ascends the auditory pathway (see complete reference list in Fig. 9 of Joris et al. 2004). Spiral ganglion neurons exhibit a lowpass modulation transfer function (MTF) with a cutoff frequency around 1 kHz for high-CF neurons. Cochlear nucleus neurons are more heterogeneous: bushy cell MTFs are also lowpass, with cutoff frequencies only slightly lower than the AN, while stellate and octopus MTFs vary, trending from lowpass to bandpass as level increases, with cutoff frequencies generally lower than those of bushy cells (Frisina et al. 1990). Inferior colliculus and auditory cortex neurons, on the other hand, have upper cutoff frequencies around 400 and 60 Hz, respectively. Therefore, at the highest modulation frequencies, EFRs should be dominated by the AN and cochlear nucleus, while at lower modulation frequencies, responses could be generated by several sources. Consistent with these predictions, anesthesia or sleep reduces EFR amplitudes at low modulation frequencies only (Pethe et al. 2001; Kuwada et al. 2002; Parthasarathy and Bartlett 2012), and lesions of the inferior colliculus reduce EFRs at 20–200 Hz modulation frequencies (Tsuzuku 1993; Kiren et al. 1994).

EFR group delay, i.e., the slope of the phase vs. modulation frequency function (Fig. 5G, H Fig. 7, *bottom*), can be used to infer the underlying generators. Kuwada et al. (2002) reported that each successive peak in rabbit EFR MTFs had a shorter group delay, suggesting a progression from central to peripheral sources with increasing modulation frequency. Here, group delays decreased above 1500 Hz to closely match the SP wave of the ABR indicating domination by IHC receptor potentials (Durrant et al. 1998). Eliminating AN (and central auditory) activity via ouabain confirmed this hypothesis (Fig. 6); EFR group delay indicated that only one source remained. However, even in intact animals, group delay varied little with modulation frequency below 1500 Hz, as reported by others (Pauli-Magnus et al. 2007), and the small changes observed were in the unexpected direction (shorter for lower frequencies).

The use of group delay to infer latency becomes complicated when multiple sources with different latencies are contributing. The addition of two sources with different latencies results in an amplitude function that fluctuates with modulation frequency and yields a delay equal to a weighted sum (by their amplitudes) of the two source delays at amplitude peaks (Shera and Bergevin 2012). Addition of more than two sources, as is generally the case in EFRs, further complicates the interpretation.

According to our effect size analysis, modulation frequencies near 1 kHz produced the most robust detection of low-SR neuropathy (Fig. 8). The decreased effect of neuropathy at lower modulation frequencies may reflect increased contribution from higher centers with less prominent noise-induced response reductions, possibly due to changes in "central gain" as suggested by prior studies of noise damage (Gu et al. 2012; Robertson et al. 2013; Schaette 2014) and by present ABR data (Fig. 9). The decreased effect of neuropathy on EFRs at higher modulation frequencies may reflect an increased contribution of hair cells, which have an even higher corner frequency than the AN (Kidd and Weiss 1990; Greenwood and Joris 1996). For most electrode configurations, the group delay near 1-kHz modulation frequency was 2 ms, i.e., similar to the latency of ABR peak II (Fig. 7, *top*), which according to lesion studies in the cat, is generated by bushy cells of the cochlear nucleus (Melcher and Kiang 1996). As argued above, such a group delay is not inconsistent with contributions from both AN and cochlear nucleus. While stellate cells contribute little to the ABR, since their modulation phase-locking is much

better than that of bushy cells and AN fibers (Frisina et al. 1990), their EFR contribution may be more substantial. However, since 1 kHz is above the upper cutoff frequency of most stellate cells, using a high modulation frequency may isolate the response to AN fibers and bushy cells.

EFRs should be most sensitive to cochlear neuropathy when using an electrode configuration that elicits a response dominated by the AN. As expected, placing an electrode closer to the cochlea increased the AN response in the ABR (Fig. 7C). However, increased SPs indicated that this configuration also increased the hair cell response, which is unaffected by noise-induced primary neural degeneration. This complicated the EFR MTF, reducing in a complex way the range of modulation frequencies sensitive to the cochlear neuropathy (Fig. 8A, purple line). Placing the electrode farther from the ear canal produced smaller overall signal amplitudes, but smoother MTFs (Fig. 7A, B, D). Although group delays indicated significant contributions from sources central to the AN, the effect size analysis suggested that the pinna to pinna configuration is the most sensitive to noise-induced cochlear neuropathy (Fig. 8). Indeed, this configuration might be expected to minimize the contribution of the symmetrically positioned inferior colliculus, and to maximize the contribution of asymmetrically positioned peripheral generators.

Detecting Low-SR Synaptopathy in Humans

The number of AN fibers per hair cell decreases with age in both mice and humans (Makary et al. 2011; Sergeyenko et al. 2013), perhaps due to accumulated noise exposure. Indeed, Individuals with a history of noise exposure, despite normal audiometric thresholds, have poorer EFRs (Plack et al. 2014; Bharadwaj et al. 2015), which may be caused by low-SR neuropathy. ABR and EFR amplitudes are reduced in aged rats, but ABR reductions are greater than predicted by changes in EFRs (Parthasarathy et al. 2014). In the present study, effects of neuropathic noise were level dependent; at high levels, reduction was greater in ABRs than EFRs, at moderate levels, reduction was greater in EFRs (Fig. 11). As discussed above, these changes are consistent with AN single-unit responses. Further exploration of the utility of ABR and EFR in teasing apart changes due to aging vs. noise exposure per se requires measurements using the same species and electrode configurations.

While a decrease in ABR or EFR amplitudes can be used to detect low-SR neuropathy in mice, in humans, the amplitudes of these evoked responses are highly variable, at least partially because of heterogeneity in head size, tissue resistance, and electrode placement: thus, diagnosis will be more difficult (Gorga et al. 1988; Nikiforidis et al. 1993). In humans, correlations between EFR amplitudes and perceptual measures can be improved by within-subject normalization (Bharadwaj et al. 2015). In the present dataset, inter-group differences were not improved by a slope transformation, possibly due to the relatively low inter-subject anatomical variations in genetically identical mice. ABR amplitudes are also more variable in outbred guinea pigs than in mice; however, they can be used for detecting cochlear neuropathy after normalizing by pre-exposure amplitudes (Furman et al. 2013). This type of normalization may also be possible in some clinical scenarios.

The present study was motivated, in part, by the idea that EFR phase measures might be more robust to heterogeneity-induced amplitude variability. Noise-induced neuropathy caused similar reductions in PLV and amplitude (Figs. 5 and 10), but PLV effect size was lower, indicating that amplitude is a more robust indicator of neuropathy in this case. However, since PLVs may be more reliable than amplitudes when signal-to-noise is poor (Zhu et al. 2013), they may be especially useful in clinical settings where extensive averaging is not possible.

Under optimized parameters, EFRs are more sensitive to neuropathy than ABRs. These optimal parameters succeed because they bias responses towards peripheral neural generators while minimizing contributions from hair cells. Optimal modulation frequency is near the high-frequency cutoff of peripheral generators (~1 kHz here) and ideal electrode configuration is one that increases ABR wave I without increasing SP. In humans, using a high modulation frequency may be especially important because it minimizes the contribution from higher centers where responses are influenced by learning (Anderson et al. 2013; Strait and Kraus 2014) and arousal levels (Kuwada et al. 2002). While responses can be measured in humans at modulation frequencies as high as 1 kHz, amplitudes are low. It is not yet clear what constitutes the best compromise. Due to differences in anatomy, optimal parameters differ between species. EFR group delay can be used to estimate EFR generators, and determine these parameters. Application of these principles in humans will improve detection of neuropathy, leading to a more refined diagnosis of sensorineural hearing loss.

ACKNOWLEDGMENTS

We thank Leslie Liberman for expert assistance in cochlear immunostaining, and Yanbo Yin and Mingjie Tong for their assistance in the ouabain experiment. We thank Andrea Meredith for providing the BK knockout mice. Research supported by grants from the National Institute on Deafness and other Communicative Disorders: R01 DC 00188 (MCL), P30 DC 05209 (MCL) and T32 DC 00038 (LAS).

REFERENCES

ANDERSON S, WHITE-SCHWOCH T, CHOI HJ, KRAUS N (2013) Training changes processing of speech cues in older adults with hearing loss. Front Syst Neurosci 7:97

AZARIAS G, KRUUSMÄGI M, CONNOR S, AKKURATOV EE, LIU X-L, LYONS D, BRISMAR H, BROBERGER C, APERIA A (2013) A specific and essential role for Na, K-ATPase α3 in neurons co-expressing α1 and α3. J Biol Chem 288:2734–2743

BHARADWAJ HM, VERHULST S, SHAHEEN L, LIBERMAN MC, SHINN-CUNNINGHAM BG (2014) Cochlear neuropathy and the coding of supra-threshold sound. Front Syst Neurosci 8:26

BHARADWAJ HM, MASUD S, MEHRAEI G, VERHULST S, SHINN-CUNNINGHAM BG (2015) Individual differences reveal correlates of hidden hearing deficits. J Neurosci 35:2161–2172

BOURIEN J, TANG Y, BATREL C, HUET A, LENOIR M, LADRECH S, DESMADRYL G, NOUVIAN R, PUEL J-L, WANG J (2014) Contribution of auditory nerve fibers to compound action potential of the auditory nerve. J Neurophysiol 112:1025–1039

CAMPBELL F, ATKINSON J, FRANCIS M, GREEN D (1977) Estimation of auditory thresholds using evoked potentials. Clin Screen Test Progr Clin Neurophysiol 2:68–78

COOPER NP, ROBERTSON D, YATES GK (1993) Cochlear nerve fiber responses to amplitude-modulated stimuli: variations with spontaneous rate and other response characteristics. J Neurophysiol 70:370–386

D'HAENENS W, DHOOGE I, MAES L, BOCKSTAEL A, KEPPLER H, PHILIPS B, SWINNEN F, VINCK BM (2009) The clinical value of the multiple-frequency 80-Hz auditory steady-state response in adults with normal hearing and hearing loss. Arch Otolaryngol Neck Surg 135:496–506

DIMITRIJEVIC A, JOHN MS, PICTON TW (2004) Auditory steady-state responses and word recognition scores in normal-hearing and hearing-impaired adults. Ear Hear 25:68–84

DOBIE RA, WILSON MJ (1989) Analysis of auditory evoked potentials by magnitude-squared coherence. Ear Hear 10:2–13

DURRANT JD, WANG J, DING DL, SALVI RJ (1998) Are inner or outer hair cells the source of summating potentials recorded from the round window? J Acoust Soc Am 104:370–377

FRISINA RD, SMITH RL, CHAMBERLAIN SC (1990) Encoding of amplitude modulation in the gerbil cochlear nucleus: I. A hierarchy of enhancement. Hear Res 44:99–122

FURMAN AC, KUJAWA SG, LIBERMAN MC (2013) Noise-induced cochlear neuropathy is selective for fibers with low spontaneous rates. J Neurophysiol 110:577–586

GORGA MP, KAMINSKI JR, BEAUCHAINE KA, JESTEADT W (1988) Auditory brainstem responses to tone bursts in normally hearing subjects. J Speech Hear Res 31:87–97

GREENWOOD DD, JORIS PX (1996) Mechanical and "temporal" filtering as codeterminants of the response by cat primary fibers to amplitude-modulated signals. J Acoust Soc Am 99:1029–1039

GU JW, HERRMANN BS, LEVINE RA, MELCHER JR (2012) Brainstem auditory evoked potentials suggest a role for the ventral cochlear nucleus in tinnitus. J Assoc Res Otolaryngol 13:819–833

HAFIDI A, BEURG M, DULON D (2005) Localization and developmental expression of BK channels in mammalian cochlear hair cells. Neuroscience 130:475–484

HALL JW (2006) New handbook for auditory evoked responses, 1st edn. Pearson, Boston

HENTSCHKE H, STÜTTGEN MC (2011) Computation of measures of effect size for neuroscience data sets. Eur J Neurosci 34:1887–1894

HERDMAN AT, LINS O, ROON PV, STAPELLS DR, SCHERG M, PICTON TW (2002) Intracerebral sources of human auditory steady-state responses. Brain Topogr 15:69–86

JOHNSON TA, BROWN CJ (2005) Threshold prediction using the auditory steady-state response and the tone burst auditory brain stem response: a within-subject comparison. Ear Hear 26:559–576

JORIS PX, YIN TC (1992) Responses to amplitude-modulated tones in the auditory nerve of the cat. J Acoust Soc Am 91:215–232

JORIS PX, SCHREINER CE, REES A (2004) Neural processing of amplitude-modulated sounds. Physiol Rev 84:541–577

KHIMICH D, NOUVIAN R, PUJOL R, TOM DIECK S, EGNER A, GUNDELFINGER ED, MOSER T (2005) Hair cell synaptic ribbons are essential for synchronous auditory signalling. Nature 434:889–894

KIDD RC, WEISS TF (1990) Mechanisms that degrade timing information in the cochlea. Hear Res 49:181–207

KIREN T, AOYAGI M, FURUSE H, KOIKE Y (1994) An experimental study on the generator of amplitude-modulation following response. Acta Oto-Laryngol Suppl 511:28–33

KUJAWA SG, LIBERMAN MC (2006) Acceleration of age-related hearing loss by early noise exposure: evidence of a misspent youth. J Neurosci 26:2115–2123

KUJAWA SG, LIBERMAN MC (2009) Adding insult to injury: cochlear nerve degeneration after "temporary" noise-induced hearing loss. J Neurosci 29:14077–14085

KUWADA S, BATRA R, MAHER VL (1986) Scalp potentials of normal and hearing-impaired subjects in response to sinusoidally amplitude-modulated tones. Hear Res 21:179–192

KUWADA S, ANDERSON JS, BATRA R, FITZPATRICK DC, TEISSIER N, D'ANGELO WR (2002) Sources of the scalp-recorded amplitude modulation following response. J Am Acad Audiol 13:188

LANG H, LI M, KILPATRICK LA, ZHU J, SAMUVEL DJ, KRUG EL, GODDARD JC (2011) Sox2 Up-regulation and glial cell proliferation following degeneration of spiral ganglion neurons in the adult mouse inner Ear. J Assoc Res Otolaryngol 12:151–171

LIBERMAN MC (1978) Auditory-nerve response from cats raised in a low-noise chamber. J Acoust Soc Am 63:442–455

LIBERMAN MC (1980) Morphological differences among radial afferent fibers in the cat cochlea: an electron-microscopic study of serial sections. Hear Res 3:45–63

LIBERMAN MC, DODDS LW, PIERCE S (1990) Afferent and efferent innervation of the cat cochlea: quantitative analysis with light and electron microscopy. J Comp Neurol 301:443–460

LIN H, FURMAN A, KUJAWA S, LIBERMAN M (2011) Primary neural degeneration in the guinea pig cochlea after reversible noise-induced threshold shift. J Assoc Res Otolaryngol 12:605–616

LOBARINAS E, SALVI R, DING D (2013) Insensitivity of the audiogram to carboplatin induced inner hair cell loss in chinchillas. Hear Res 302:113–120

MAISON SF, PYOTT SJ, MEREDITH AL, LIBERMAN MC (2013a) Olivocochlear suppression of outer hair cells in vivo: evidence for combined action of BK and SK2 channels throughout the cochlea. J Neurophysiol 109:1525–1534

MAISON SF, USUBUCHI H, LIBERMAN MC (2013b) Efferent feedback minimizes cochlear neuropathy from moderate noise exposure. J Neurosci 33:5542–5552

MAKARY C, SHIN J, KUJAWA S, LIBERMAN M, MERCHANT S (2011) Age-related primary cochlear neuronal degeneration in human temporal bones. J Assoc Res Otolaryngol 12:711–717

MATSUBARA A, LAAKE JH, DAVANGER S, USAMI S, OTTERSEN OP (1996) Organization of AMPA receptor subunits at a glutamate synapse: a quantitative immunogold analysis of hair cell synapses in the rat organ of Corti. J Neurosci 16:4457–4467

MELCHER JR, KIANG NYS (1996) Generators of the brainstem auditory evoked potential in cat III: identified cell populations. Hear Res 93:52–71

MEREDITH AL, THORNELOE KS, WERNER ME, NELSON MT, ALDRICH RW (2004) Overactive bladder and incontinence in the absence of the BK large conductance Ca2+–activated K+ channel. J Biol Chem 279:36746–36752

Müller M, von Hünerbein K, Hoidis S, Smolders JWT (2005) A physiological place–frequency map of the cochlea in the CBA/J mouse. Hear Res 202:63–73

Nikiforidis GC, Koutsojannis CM, Varakis JN, Goumas PD (1993) Reduced variance in the latency and amplitude of the fifth wave of auditory brain stem response after normalization for head size. Ear Hear 14:423–428

Obrien WJ, Lingrel JB, Wallick ET (1994) Ouabain binding kinetics of the rat alpha two and alpha three isoforms of the sodium-potassium adenosine triphosphate. Arch Biochem Biophys 310:32–39

Oliver D, Taberner AM, Thurm H, Sausbier M, Arntz C, Ruth P, Fakler B, Liberman MC (2006) The role of BKCa channels in electrical signal encoding in the mammalian auditory periphery. J Neurosci 26:6181–6189

Parthasarathy A, Bartlett E (2012) Two-channel recording of auditory-evoked potentials to detect age-related deficits in temporal processing. Hear Res 289:52–62

Parthasarathy A, Datta J, Torres JAL, Hopkins C, Bartlett EL (2014) Age-related changes in the relationship between auditory brainstem responses and envelope-following responses. J Assoc Res Otolaryngol 15:649–661

Pauli-Magnus D, Hoch G, Strenzke N, Anderson S, Jentsch TJ, Moser T (2007) Detection and differentiation of sensorineural hearing loss in mice using auditory steady-state responses and transient auditory brainstem responses. Neuroscience 149:673–684

Pethe J, Von Specht H, Mühler R, Hocke T (2001) Amplitude modulation following responses in awake and sleeping humans—a comparison for 40 Hz and 80 Hz modulation frequency. Scand Audiol Suppl 152–155

Ping J, Li N, Du Y, Wu X, Li L, Galbraith G (2007) Auditory evoked responses in the rat: transverse mastoid needle electrodes register before cochlear nucleus and do not reflect later inferior colliculus activity. J Neurosci Methods 161:11–16

Plack CJ, Barker D, Prendergast G (2014) Perceptual consequences of "hidden" hearing loss. Trends Hear 18

Pyott SJ, Meredith AL, Fodor AA, Vázquez AE, Yamoah EN, Aldrich RW (2007) Cochlear function in mice lacking the BK channel α, β1, or β4 subunits. J Biol Chem 282:3312–3324

Rhode WS, Smith PH (1985) Characteristics of tone-pip response patterns in relationship to spontaneous rate in cat auditory nerve fibers. Hear Res 18:159–168

Rickards FW, Clark GM (1972) Field potentials in cat auditory nuclei in response to frequency and amplitude modulated sound. Proc Aust Physiol Pharmacol Soc p 201

Robertson D, Bester C, Vogler D, Mulders WHAM (2013) Spontaneous hyperactivity in the auditory midbrain: relationship to afferent input. Hear Res 295:124–129

Ruggles D, Bharadwaj H, Shinn-Cunningham BG (2011) Normal hearing is not enough to guarantee robust encoding of suprathreshold features important in everyday communication. Proc Natl Acad Sci U S A 108:15516–15521

Sausbier U, Sausbier M, Sailer CA, Arntz C, Knaus H-G, Neuhuber W, Ruth P (2006) Ca2+–activated K+ channels of the BK-type in the mouse brain. Histochem Cell Biol 125:725–741

Schaette R (2014) Tinnitus in men, mice (as well as other rodents), and machines. Hear Res 311:63–71

Schmiedt RA, Okamura H-O, Lang H, Schulte BA (2002) Ouabain application to the round window of the gerbil cochlea: a model of auditory neuropathy and apoptosis. J Assoc Res Otolaryngol 3:223–233

Schwaber MK, Hall JW (1990) A simplified technique for transtympanic electrocochleography. Am J Otol 11:260–265

Sergeyenko Y, Lall K, Liberman MC, Kujawa SG (2013) Age-related cochlear synaptopathy: an early-onset contributor to auditory functional decline. J Neurosci 33:13686–13694

Shera CA, Bergevin C (2012) Obtaining reliable phase-gradient delays from otoacoustic emission data. J Acoust Soc Am 132:927–943

Skinner LJ, Enée V, Beurg M, Jung HH, Ryan AF, Hafidi A, Aran J-M, Dulon D (2003) Contribution of BK Ca2+–activated K+ channels to auditory neurotransmission in the guinea Pig cochlea. J Neurophysiol 90:320–332

Stamataki S, Francis HW, Lehar M, May BJ, Ryugo DK (2006) Synaptic alterations at inner hair cells precede spiral ganglion cell loss in aging C57BL/6J mice. Hear Res 221:104–118

Stapells DR, Makeig S, Galambos R (1987) Auditory steady-state responses: threshold prediction using phase coherence. Electroencephalogr Clin Neurophysiol 67:260–270

Strait DL, Kraus N (2014) Biological impact of auditory expertise across the life span: musicians as a model of auditory learning. Hear Res 308:109–121

Taberner AM (2005) Using knockout mice to study the molecular mechanisms that shape auditory nerve responses. Dissertation, Massachusetts Institute of Technology

Taberner AM, Liberman MC (2005) Response properties of single auditory nerve fibers in the mouse. J Neurophysiol 93:557–569

Tsuzuku T (1993) 40-Hz steady state response in awake cats after bilateral chronic lesions in auditory cortices or inferior Colliculi. Auris Nasus Larynx 20:263–274

Yuan Y, Shi F, Yin Y, Tong M, Lang H, Polley DB, Liberman MC, Edge ASB (2014) Ouabain-induced cochlear nerve degeneration: synaptic loss and plasticity in a mouse model of auditory neuropathy. J Assoc Res Otolaryngol 15:31–43

Zhu L, Bharadwaj H, Xia J, Shinn-Cunningham B (2013) A comparison of spectral magnitude and phase-locking value analyses of the frequency-following response to complex tones. J Acoust Soc Am 134:384–395